A wide-angle dual-band infrared perfect absorber based on metal–dielectric–metal split square-ring and square array

2012 J. Phys. D: Appl. Phys. 45 205101

(http://iopscience.iop.org/0022-3727/45/20/205101)

IOP PUBLISHING JOURNAL OF PHYSICS D: APPLIED PHYSICS

J. Phys. D: Appl. Phys. **45** (2012) 205101 (6pp) doi:10.1088/0022-3727/45/20/205101

A wide-angle dual-band infrared perfect absorber based on metal–dielectric–metal split square-ring and square array

H M Lee[1,2] **and J C Wu**[1]

[1] Department of Physics, National Changhua University of Education, Changhua 500, Taiwan
[2] Institute of Physics, National Chiao Tung University, Hsinchu 300, Taiwan

E-mail: phjcwu@cc.ncue.edu.tw

Received 6 February 2012, in final form 21 March 2012
Published 1 May 2012
Online at stacks.iop.org/JPhysD/45/205101

Abstract
The optical properties of a dual-band plasmonic absorber are delineated numerically by employing a finite element method. Based on a metal–dielectric–metal scheme, the key structure consists of a lossless dielectric layer that is sandwiched by a silver split square-ring enclosing a silver square array and ground silver plane. The simulation results clearly show that near-perfect absorption efficiency can be realized for two absorption bands in the near-infrared wavelength range. The near-perfect absorption bands exhibit polarization insensitivity and wide-angle incidence. Notably, the absorption band is independently governed by the size of each part of the patterned films where the silver split square-ring determines the shorter wavelength band and the silver square determines the longer wavelength band, respectively. The repositioning of two near-perfect absorption peaks possesses a linear relationship that is related to the dimensions of the patterned silver layer. This allows for a flexible reconfigurability over the entire near-infrared regime.

(Some figures may appear in colour only in the online journal)

1. Introduction

Artificial plasmonic nanostructures have drawn a surge of interest over the past several years because of their exotic electromagnetic responses in negative refraction, superlensing and cloaking [1–4]. These metallic composite devices can be characterized by an effective medium technique [5] with complex permittivity and permeability. While much effort has been devoted to developing low-loss negatively reflecting materials, it has recently been shown that near-perfect absorption is possible by improving the design of metal–dielectric nanostructures [6]. Indeed, plasmonic nanostructures with near-perfect absorption bands are highly desirable for many versatile applications including metamaterial absorbers [6–20], photovoltaic cells [21–23], sensors [24–26], photodetectors [27, 28], thermal emitters [29, 30] and optical imaging devices [31–33].

To realize near-perfect absorption, the plasmonic nanostructures are usually engineered by simultaneously minimizing the reflectance with perfect impedance matching and eliminating the transmittance by maximizing material losses [6–10, 17–20, 25]. Among these plasmonic nanostructures, the metal–dielectric–metal based absorbers (MDM absorbers) have shown promising potential because of near-perfect absorptive efficiency, wide-angle incidence properties and an almost complete lack of sensitivity to polarization [9, 17–20, 25]. MDM absorbers typically consist of three functional layers that comprise a dielectric layer sandwiched between two metal layers. The top layer is mainly a periodically patterned metallic nanostructure that serves as an electric resonator. The bottom layer is mostly the thick metal plane which is used as an optical mirror that significantly reduces transmittance. The coupling between two metallic layers results in magnetic resonance depending on the thickness and dielectric constant of the dielectric layer [17]. To date, the near-perfect MDM absorbers have been investigated from microwave to optical frequencies with single-band [9, 17, 25], dual-band [18], triple-band [20] and broad-band [19] absorptions. For the near-infrared wavelength range, single-band MDM absorbers [17, 25] exhibit near-perfect absorption,

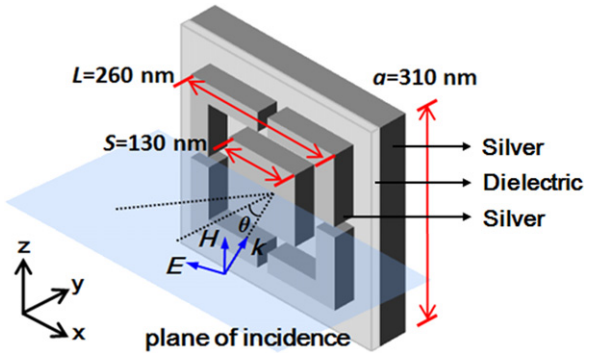

Figure 1. Schematic drawing of the dual-band MDM absorber structure and the incident TM polarization wave.

polarization insensitivity and wide-angle incidence. However, they merely operate at a specific frequency band. This fact strictly limits their use in applications such as spectroscopic detection and imaging which requires the resolution of distinct absorption features at multiple frequencies [34]. Thus, multi-band near-infrared absorbers with two [35] or more [36] optimized absorption bands are in demand. Zhang *et al* have recently demonstrated a dual-band near-infrared absorber that is based on an elliptical nanodisc MDM array [18]. Their dual-band design shows the characteristics of near-perfect absorption, wide-angle incidence, and polarization independence in the near-infrared wavelength range. Although two absorption peaks of their absorber can be adjusted by varying the dimensions of the elliptical nanodiscs, they are always shifted together, i.e. either red-shifted, blue-shifted, toward-shifted or outward-shifted simultaneously for two absorptions. The two absorption peaks cannot be adjusted individually. To have arbitrary dual-band absorptions over the entire near-infrared range, one needs to reconsider a brand new MDM structure which has more flexible reconfigurability.

In this paper, a dual-band plasmonic absorber that is based on an MDM structure is numerically studied. The proposed dual-band MDM absorber shows wide-angle incidence, polarization insensitivity and near-perfect absorption bands in the near-infrared wavelength range. Notably, the two absorption peaks of the absorber can be individually tuned by adjusting the dimensions of the MDM structures which makes this dual-band absorber more attractive when it comes to designing a near-infrared near-perfect absorption device.

2. Simulation structure and methods

The designed MDM absorber is numerically delineated by employing a commercially available RF package that uses a finite element method [37]. The MDM structures which are periodically arranged in a cubically latticed pattern on the x–z plane can be effectively reduced to a simple modelling unit cell as shown in figure 1. A 10 nm thick dielectric layer is sandwiched between two thick silver metallic layers. The thickness of the dielectric layer that vitally affects the dipolar resonance between the two metal layers has been optimized to achieve the near-perfect absorption efficiency [17]. The patterned silver layer with a thickness of 40 nm consists of a split square-ring and a square with side lengths denoted as L and S, respectively. The line width and split gap of the split square-ring and period a of the unit cell are kept constant at 30 nm, 20 nm and 310 nm, respectively, for all the following simulations. The ground silver layer with a thickness of 50 nm has two significant functions. The first function is to serve as an optical mirror with a thickness that is greater than the penetration depth of the incident light in the near-infrared wavelength range in order to minimize the transmittance further towards zero. The second function is to couple with the silver split square-ring and square array to create electric and magnetic dipoles which dramatically concentrate electromagnetic energy into the MDM structure. Thus, the absorbance is characterized as $A = 1 - R$, where R denotes the reflectance.

In this simulation, we use Floquet boundary conditions and perfect matched layers with sufficient grid numbers to perform the calculation [39, 40]. The complex dielectric function of silver is interpolated by fitting the data to the curve in Palik's handbook [38] while the refractive index of the dielectric layer is set to a constant of 1.53. Two polarized plane waves are used to examine the absorptive properties of the dual-band absorber. As shown in figure 1, the transverse magnetic (TM) polarized wave with an orientation of electric (E), magnetic (H) and propagation (k) vectors is illuminated on the MDM absorber with an incident angle of θ. Opposite to the TM wave, the E of the transverse electric one (TE) is perpendicular to the plane of incidence with H lying on the plane. The dual-band absorptions are then calculated in the near-infrared range with wavelength λ ranging from 1000 to 2000 nm and θ ranging up to 90°.

3. Results and discussion

As stated previously, the dual-band MDM absorber consists of two metallic layers separated by a lossless dielectric layer. The patterned silver layer that is composed of a split square-ring and square array is responsible for electric dipolar resonances while the ground silver plane layer is mainly used for creating magnetic dipolar resonances between the two metallic layers. Additionally, the two absorption peaks can be attributed to the combinatorial effect of the individual dipolar resonances from each of the split square-ring [9] and square [17]. Thus, we first optimize two single-band absorbers at normally incident TM (or TE) plane wave as shown in figure 2. The blue solid curve represents near-perfect absorption from the square pattern alone at $S = 130$ nm, while the red one again shows near-perfect absorption coming from the split square-ring pattern at $L = 260$ nm. When the results of the split square-ring and square patterns are taken as a whole, two near-perfect absorption bands are obtained at $\lambda = 1160$ nm ($A = 100\%$) and $\lambda = 1585$ nm ($A = 99\%$), respectively, as shown by the black solid curve in figure 2. The following simulations further determine whether the dual-band absorber holds the properties of polarization insensitivity, wide-angle incidence and flexible reconfigurability for two absorption bands.

Figure 3 shows the absorbance as a function of both wavelength and angle of incidence under TM and TE waves.

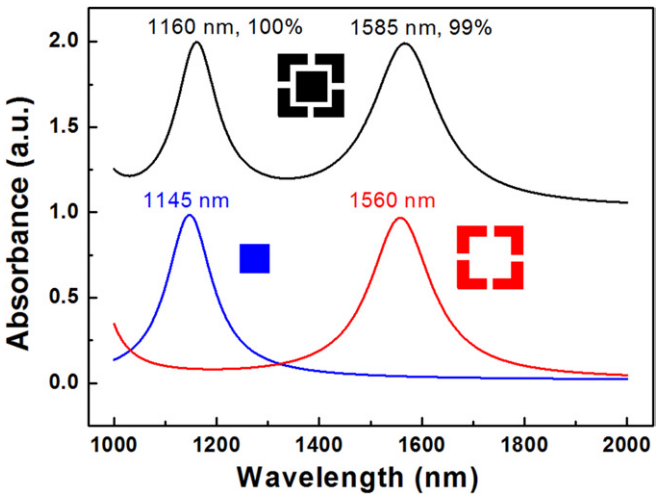

Figure 2. Absorbance spectra under normally incident TM (or TE) plane wave. The blue/red/black solid curves represent the absorbance spectra for silver square, silver split square-ring and the combined structure, respectively, where $L = 260$ nm, $S = 130$ nm.

For the TM case as illustrated in figure 3(a), the maximum absorption peaks for two bands remain 99% with θ up to 80°. Furthermore, the two absorption peaks become broader and exhibit blue-shift as θ becomes greater than 45°. This is quite consistent with the reported single-band MDM absorber [17] where blue-shift is also observed in the TM case. Nevertheless, for the TE one, the maximum absorption peaks with efficiency remaining at greater than 90% for two peaks dramatically decrease as θ becomes greater than 45°, especially for the one located at $\lambda = 1585$ nm, which is generated by the split square-ring pattern. Contrasting with the TM case, the bandwidth of the TE one becomes narrower as θ increases; absorbance vanishes as θ increases up to 80°. To sum up, the designed MDM absorber displays the traits of polarization insensitivity and wide-angle incidence when θ is smaller than 45°.

To disclose the physical origin of the near-perfect absorptions in this dual-band MDM absorber, the electromagnetic near-field distributions for two resonant modes ($\lambda = 1160$ nm and 1585 nm) are elucidated. Figures 4(a) and (d) present the amplitude of the magnetic field (H_y) in the x–z plane through the middle of the dielectric layer that is illuminated under the TM wave at normal incidence. Apparently, for $\lambda = 1160$ nm, a strong magnetic resonance is formed between the silver square and the ground silver plane. For $\lambda = 1585$ nm, however, strong magnetic resonances are created between the split square-ring and the ground silver plane. The two absorption bands are indeed dominated by the dimensions of the metallic split square-ring and square [41].

In order to better understand the dipolar resonances, we took the cross-sectional plots along the red dotted lines, as indicated in figures 4(a) and (d). The corresponding cross-sectional near-field profiles are shown in figures 4(b) and (e), in which the colour maps represent the amplitude of the magnetic field (H_y) and the white arrows represent the electric displacement vectors. The electric displacement vectors in both the patterned silver layer and the ground silver plane are opposite to each other. The anti-parallel displacement vectors

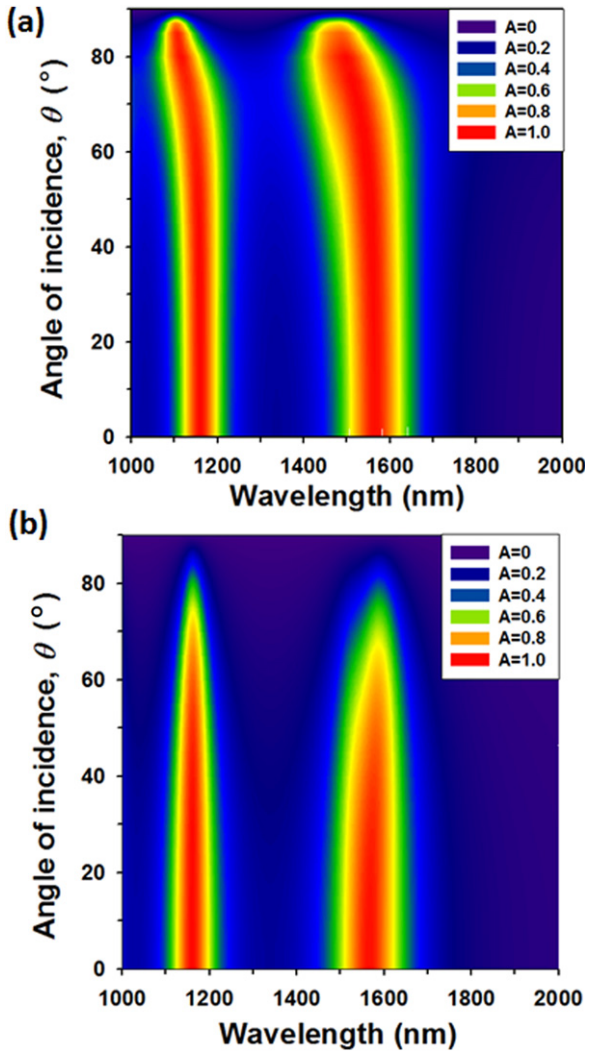

Figure 3. Contour plots of absorbance as a function of wavelength and the angle of incidence for (a) TM and (b) TE polarization plane wave. The dimensions of the dual-band absorber are the same as that in figure 2.

create circulating currents between two metal layers, resulting in an artificial magnetic moment that interacts strongly with the magnetic field of the incident light [42]. The strong magnetic dipolar resonances that result from this interaction are then excited between the two metal layers to yield two resonant modes. Moreover, the electric field distributions in the same cross-sectional profiles along both the square and split square-ring at the resonant wavelengths are plotted in figures 4(c) and (f). For the resonant peak at $\lambda = 1160$ nm, the enhanced electric fields are confined to the space between the silver square and the ground silver plane. However, for the resonant peak at $\lambda = 1585$ nm, the enhanced electric fields are confined to the space between the split gap and the space between the silver split square-ring and the ground silver plane. The strong confinement of the electric fields is what creates electric dipolar resonances. The enhanced electric fields are then transformed into heat by the Ohmic losses within the patterned and ground silver layer [17]. Therefore, the near-perfect absorption bands in our dual-band absorber are due to the MDM design that permits the excitation of localized magnetic and electric dipolar resonances.

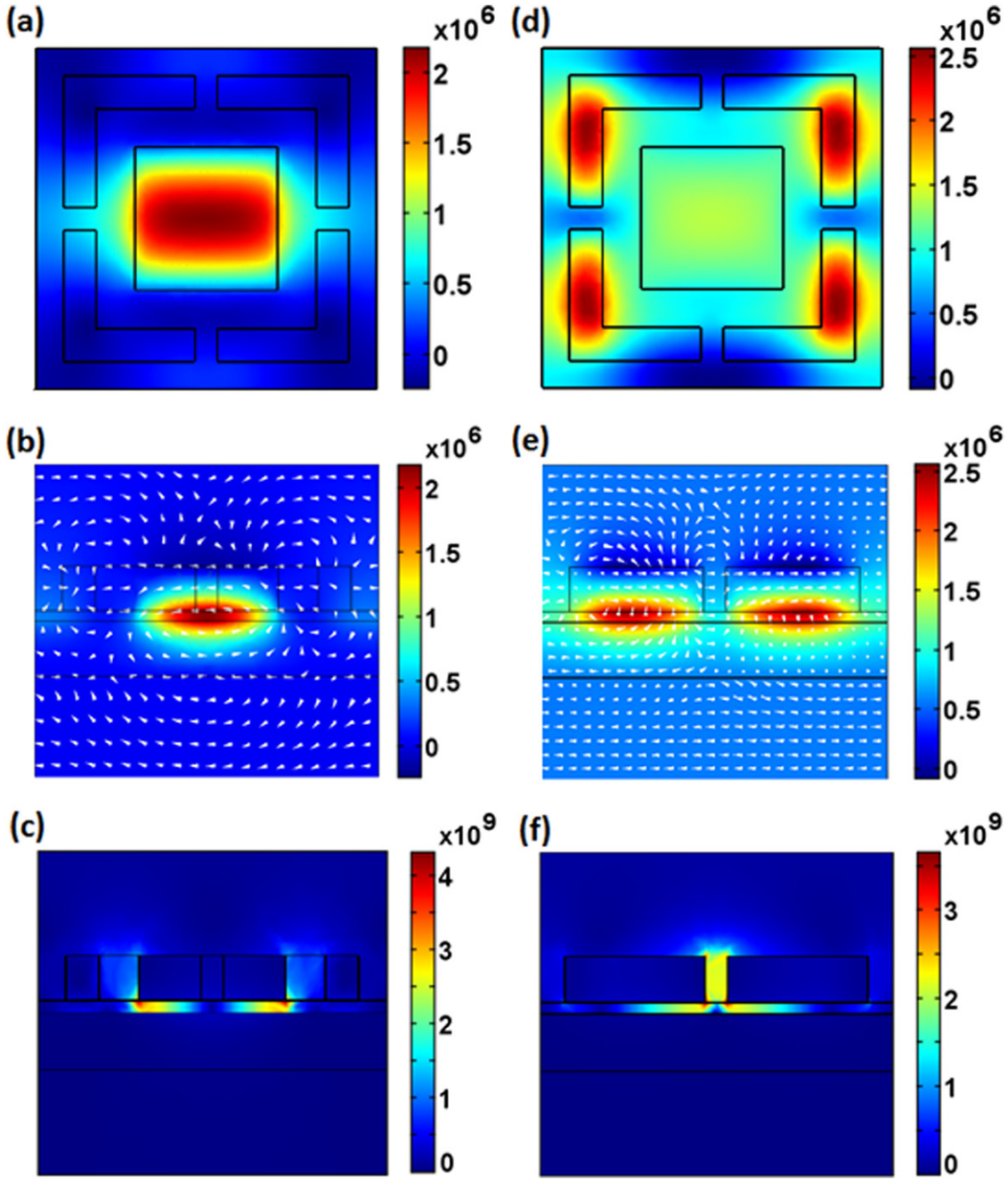

Figure 4. (*a*), (*d*) Amplitude of magnetic field (H_y) in the x–z plane through the middle of the dielectric layer at $\lambda = 1160$ and 1585 nm illuminated under normally incident TM wave; (*b*), (*e*) amplitude of the magnetic field (H_y) and the electric displacement vectors in the cross-sectional profile along the red dotted curves; (*c*), (*f*) the corresponding normalized electric field. The dimensions of the dual-band absorber are the same as those in figure 2.

After exploring the physical phenomenon through near-field profiles, the dual-band MDM absorber is further examined by changing the dimensions of the patterned silver layer. Figure 5(*a*) shows the absorbance as a function of both λ and S at normally incident TM (or TE) plane wave. S is varied from 105 nm to 165 nm while keeping $L = 260$ nm. Obviously, the leftmost absorption band at $\lambda = 1000$ nm governed by the dimension of the square can be tuned independently and linearly as it approaches the rightmost absorption band at $\lambda = 1585$ nm while keeping the rightmost absorption band almost unchanged. Increasing the size of the silver square leads to a red-shift of the absorption peak because of the red-shift of the plasmonic resonance. This repositioning of the two absorption bands is evidently different from that found in the elliptical nanodisc MDM array [18]. The tunable range of the leftmost absorption peak in this case is modelled up to 400 nm without changing a. Figure 5(*b*) exhibits the absorbance as a function of both λ and L at normally incident TM (or TE) plane wave. L is varied from 200 to 290 nm while keeping $S = 110$ nm. Once again, the leftmost absorption band remains almost unchanged while the rightmost absorption and at $\lambda = 1200$ nm, related to the split square-ring, exhibits linear red-shift up to $\lambda = 1800$ nm as L increases to 290 nm. The tunable range of the rightmost absorption peak is delineated up to 600 nm. The

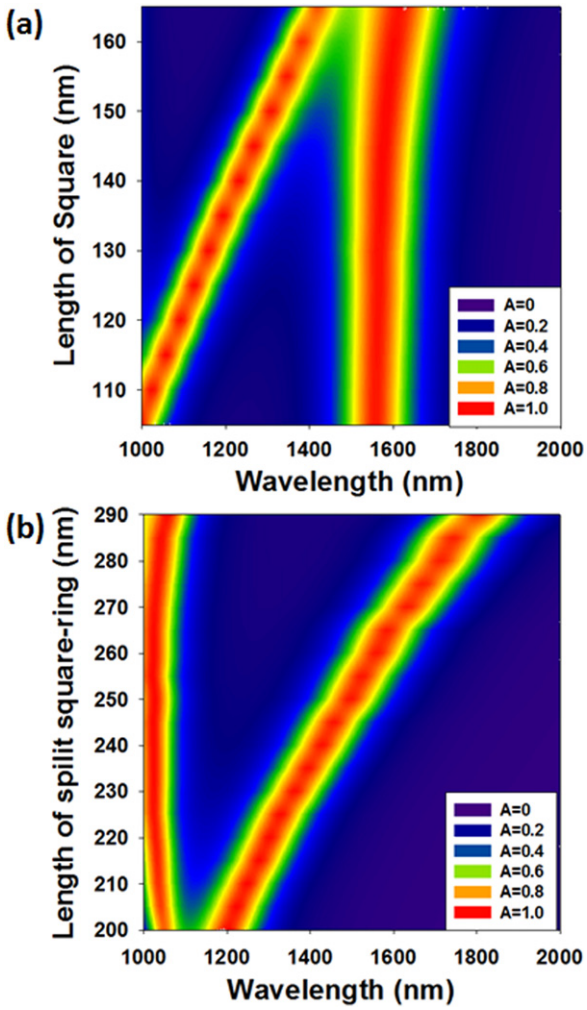

Figure 5. Contour plots of absorbance as a function of both wavelength and side length of (*a*) square S and (*b*) split square-ring L. For case (*a*), S is varied from 105 to 165 nm with fixed $L = 260$ nm. For case (*b*), L is varied from 200 to 290 nm with fixed $S = 110$ nm. The tunable ranges of two absorption peaks by separately changing S and L are modelled up to 400 nm and 600 nm, respectively.

manipulations of two absorption peaks reveal that this dual-band MDM absorber shows flexible reconfigurability with two near-perfect absorption bands that can be individually adjusted over the entire near-infrared regime.

4. Conclusion

In summary, we have numerically delineated the absorption characteristics of a dual-band MDM absorber in the near-infrared wavelength regime. The MDM structure comprises a 10 nm thick dielectric layer sandwiched by a 40 nm thick silver patterned layer that consists of a split square-ring and square array and a 50 nm thick silver plane. Two near-perfect absorption bands at $\lambda = 1160$ nm ($A = 100\%$) and $\lambda = 1585$ nm ($A = 99\%$) are obtained at normally incident TM (or TE) wave when $L = 260$ nm and $S = 130$ nm. The dual-band MDM absorber with absorbance greater than 90% exhibits polarization insensitivity and wide-angle incidence as θ increases up to 45°. Moreover, the ranges of two absorption peaks, which can be tuned separately by changing S and L, are modelled up to 400 nm and 600 nm, respectively, without optimizing a. The ability to reconfigure two absorption bands individually by adjusting the dimensions of the MDM structures makes our dual-band absorber more attractive when it comes to designing near-infrared perfect absorption devices such as metamaterial absorbers, solar cells, sensors, photodetectors and thermal emitters.

Acknowledgments

The authors acknowledge the support from the National Science Council of the Republic of China under Grant numbers of NSC98-2811-M-018-012, NSC100-2120-M-009-008 and NSC98-2112-M-018-004-MY3.

References

[1] Smith D R, Padilla W J, Vier D C, Nemat-Nasser S C and Schultz S 2000 *Phys. Rev. Lett.* **84** 4184
[2] Smith D R, Pendry J B and Wiltshire M C K 2004 *Science* **305** 788
[3] Leonhardt U 2006 *Science* **312** 1777
[4] Pendry J B, Schurig D and Smith D R 2006 *Science* **312** 1780
[5] Smith D R and Pendry J B 2006 *J. Opt. Soc. Am.* B **23** 391
[6] Landy N I, Sajuyigbe S, Mork J J, Smith D R and Padilla W J 2008 *Phys. Rev. Lett.* **100** 207402
[7] Yen T J, Padilla W J, Fang N, Vier D C, Smith D R, Pendry J B, Basov D N and Zhang X 2004 *Science* **303** 1494
[8] Tao H, Landy N I, Bingham C M, Zhang X, Averitt R D and Padilla W J 2008 *Opt. Express* **16** 7181
[9] Tao H, Bingham C M, Strikwerda A C, Pilon D, Shrekenhamer D, Landy N I, Fan K, Zhang X, Padilla W J and Averitt R D 2008 *Phys. Rev.* B **78** 241103(R)
[10] Landy N I, Bingham C M, Tyler T, Jokerst N, Smith D R and Padilla W J 2009 *Phys. Rev.* B **79** 125104
[11] Radooru Y R, Yakovlev A B, Kaipa C S R, Medina F and Mesa F 2011 *Phys. Rev.* B **84** 035108
[12] Avitzour Y, Urzhumov Y A and Shvets G 2009 *Phys. Rev.* B **79** 045131
[13] Argyropoulos C, Kallos E, Zhao Y and Hao Y 2009 *Opt. Express* **17** 8467
[14] Jack N, Chen H Y and Chan C T 2009 *Opt. Lett.* **34** 644
[15] Ishikawa A, Zhang S, Genov D A, Bartal G and Zhang X 2009 *Phys. Rev. Lett.* **102** 043904
[16] Xiao S, Chettiar U K, Kildishev A V, Drachev V, Khoo I C and Shalaev V M 2009 *Appl. Phys. Lett.* **95** 033115
[17] Hao J, Wang J, Liu X, Padilla W J, Zhou L and Qiu M 2010 *Appl. Phys. Lett.* **96** 251104
[18] Zhang B, Zhao Y, Hao Q, Kiraly B, Iam-Choon Khoo, Chen S and Huang T J 2011 *Opt. Express* **19** 15221
[19] Aydin K, Ferry V E, Briggs R M and Atwater H A 2011 *Nature Commun.* **2** 517
[20] Shen X, Cui T J, Zhao J, Ma H F, Jiang W X and Li H 2011 *Opt. Express* **19** 9401
[21] Nakayama K, Tanabe K and Atwater H A 2008 *Appl. Phys. Lett.* **93** 121904
[22] Catchpole K R and Polman A 2008 *Opt. Express* **16** 21793
[23] Munday J N and Atwater H A 2011 *Nano Lett.* **11** 2195
[24] Zhu S, Li F, Du C and Fu Y 2008 *Sens. Actuators* B **134** 193
[25] Liu N, Mesch M, Weiss T, Hentschel M and Giessen H 2010 *Nano Lett.* **10** 2342
[26] Hao Q, Juluri B K, Zheng Y B, Wang B, Chiang I, Jensen L, Crespi V, Eklund P C and Huang T J 2010 *J. Phys. Chem.* C **114** 18059

[27] Yu Z, Veronis G, Fan S and Brongersma M L 2006 *Appl. Phys. Lett.* **89** 151116
[28] Rosenberg J, Shenoi R V, Vandervelde T E, Krishna S and Painter O 2009 *Appl. Phys. Lett.* **95** 161101
[29] Zheng Y B, Huang T J, Desai A Y, Wang S J, Tan L K, Gao H and Huan A C H 2007 *Appl. Phys. Lett.* **90** 183117
[30] Diem M, Koschny T and Soukoulis C M 2009 *Phys. Rev.* B **79** 033101
[31] Liu Z, Durant S, Lee H, Pikus Y, Xiong Y, Sun C and Zhang X 2007 *Opt. Express* **15** 6947
[32] Hu H, Ma C and Liu Z 2010 *Appl. Phys. Lett.* **96** 113107
[33] Zhao Y, Lin S C, Nawaz A A, Kiraly B, Hao Q, Liu Y and Huang T J 2010 *Opt. Express* **18** 23458
[34] Bandara S V, Gunapala S D, Liu J K, Rafol S B, Hill C J, Ting D Z, Mumolo J M and Trinh T Q 2005 *Infrared Phys. Technol.* **47** 15
[35] Jiang Z H, Yunt S, Toor F, Werner D H and Mayer T S 2011 *ACS Nano* **5** 4641
[36] Turkmen M, Aksu S, Cetin A E, Yanik A A and Altug H 2011 *Opt. Express* **19** 7921
[37] COMSOL RF module user's guide 2012 http://www.comsol.com.tw
[38] Palik E D 1985 *Handbook of Optical Constants of Solids* (New York: Academic)
[39] Lee H M, Horng L and Wu J C 2011 *J. Phys. D: Appl. Phys.* **44** 064016
[40] Lee H M, Shyu J H, Horng L and Wu J C 2011 *J. Vac. Sci. Technol.* B **29** 04D105
[41] Willets K A and Van Duyne R P 2007 *Annu. Rev. Phys. Chem.* **58** 267
[42] Cai W, Chettiar U K, Yuan H K, de Silva V C, Kildishev A V, Drachev V P and Shalaev V M 2007 *Opt. Express* **15** 3333